Stabilized single-frequency sub-kHz linewidth Brillouin fiber laser cavity operating at 1 μm

Moise Deroh, Erwan Lucas, Kamal Hammani, Guy Millot, Bertrand Kibler

Stabilized single-frequency sub-kHz linewidth Brillouin fiber laser cavity operating at 1 µm

MOISE DEROH[1,*], ERWAN LUCAS[1], KAMAL HAMMANI[1], GUY MILLOT[1,2], AND BERTRAND KIBLER[1]

[1] Laboratoire Interdisciplinaire Carnot de Bourgogne, UMR 6303 CNRS, Université de Bourgogne (UB), Dijon, France
[2] Institut Universitaire de France (IUF), 1 Rue Descartes, Paris, France
[*] Corresponding author: koffi.deroh@u-bourgogne.fr

Compiled October 31, 2023

We experimentally demonstrate a stabilized single-frequency Brillouin fiber laser operating at 1.06 µm by means of a passive highly nonlinear fiber (HNLF) ring cavity combined with a phase-locking loop scheme. The stimulated Brillouin scattering efficiency is first investigated in distinct single-mode germanosilicate core fibers with increasing GeO_2 content. The most suitable fiber, namely 21 mol.% GeO_2 core fiber, is used as Brillouin gain medium in the laser cavity made with a 15-m-long-segment. A Stokes lasing threshold of 140 mW is reported. We also show significant linewidth narrowing (below 1-kHz) as well as frequency noise reduction compared to that of the initial pump in our mode-hop free Brillouin fiber laser.

http://dx.doi.org/10.1364/ao.XX.XXXXXX

1. INTRODUCTION

Stimulated Brillouin Scattering (SBS) in optical waveguides is a nonlinear effect that occurs when the optical field interacts with acoustic waves through electrostriction and photo-elastic phenomena [1, 2]. Several studies based on the SBS process have been extensively demonstrated for many important applications [3–7]. Among these, we distinguish the Brillouin lasers which have attracted significant interest as ultra-high coherence light sources with sub-Hertz linewidth in simple all-fiber passive optical cavities [8] and in high-Q microresonators [9, 10] suitable for applications in optical communications and LIDAR systems. To date, most of Brillouin lasers have been designed to operate in the telecom bands. However, there is a need to develop narrow-linewidth, low-noise and high-power laser sources at shorter wavelengths for applications covering this spectral region such as sensing, high-resolution metrology and development of space-embarked systems, for inter-satellite and satellite to ground communications [11–13].

So far, only a few studies on Brillouin fiber lasers (BFLs) have been reported around 1 µm. For instance, Wang *et al.* reported a high-power all-fiber cavity laser with high slope efficiency at 1 µm wavelength [14]. In particular, they showed a single-frequency BFL of 3 kHz operating at a maximum output power of 1.4 W. Very recently, Tao *et al.* demonstrated a high-power single-polarization, single-frequency 1064 nm BFL based on a larger mode area polarization-maintaining fiber [15]. A maximum output BFL power of 4.9 W was achieved, while the linewidth was 170 kHz. In the same way, a high-power all-polarization-maintaining hybrid Brillouin/ytterbium fiber laser operating at 1064 nm was demonstrated by adopting large-mode-area fiber with core/cladding diameter of 20/400 µm [16]. Single-frequency BFL with a record output power of 23 W was achieved. However, these Brillouin laser did not present a very marked linewidth narrowing compared to the pump, and stabilization schemes for mode-hopping suppression were not implemented.

In this paper, we demonstrate a stabilized single-frequency Brillouin laser operating around 1-µm based on a highly-nonlinear germanosilicate fiber as the Brillouin gain medium. First, we characterize SBS at 1-µm pump wavelength in three distinct doped-core optical fibers with increasing GeO_2 content. Our results clearly reveal an enhancement of the Brillouin gain efficiency in heavily GeO_2 core-doped fibers compared to that of standard silica single-mode fibers. The Brillouin frequency shift (BFS) can be tuned over more than 4 GHz with a strong decrease from 15.95 GHz (SMF-28) down to 11.87 GHz (ultra-high doping level, 75 mol.% GeO_2). At the same time, the spectral width of the Brillouin gain widens strongly up to 69.7 MHz, with the increase of the GeO_2 core content. Next, we select the most suitable fiber to form our 1-µm BFL combined with a phase-locking loop scheme to ensure stable and mode-hop free operation. Owing to the intrinsic properties of SBS, a Stokes lasing threshold and narrow-linewidth of 140 mW and 50 Hz respectively, have been obtained for a 15-m-long cavity. Finally, we show a frequency noise reduction of the lasing Stokes component, compared to that of the initial pump laser source.

2. EXPERIMENTAL SETUP

Figure 1 depicts the complete experimental setup used for both implementation and characterization of our stabilized BFL with a standard non-resonant pumping configuration [4]. An amplified narrow-linewidth continuous-wave laser tunable from 1.039 to 1.075 µm (Toptica DLC-PRO-025563) was used as a

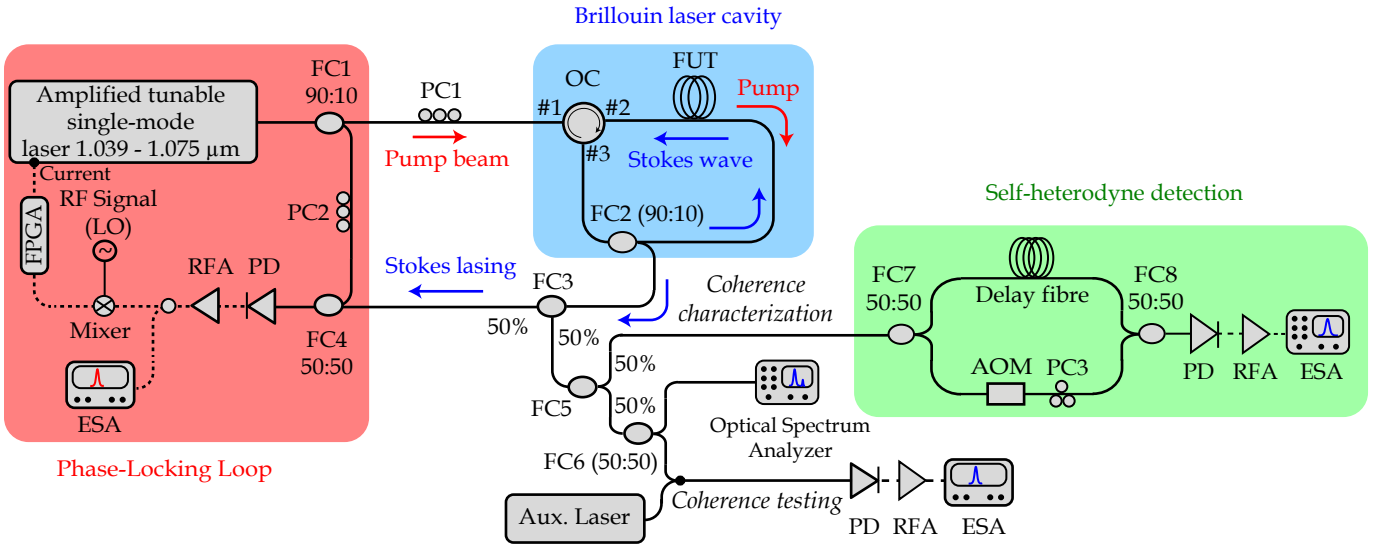

Fig. 1. Experimental setup of BFL cavity (blue rectangle) combined with a phase-locked stabilization loop diagram (red rectangle). A self-delayed heterodyne detection (green rectangle) is used here for coherence characterization of the laser. PC: Polarization controller, OC: Optical circulator, FC: Fiber coupler, FUT: Fiber under test, RFA: Radio-frequency amplifier, ESA: Electrical spectrum analyzer, PD: Photodiode, LO: Local oscillator, FPGA: Field-programmable gate array, AOM: Acousto-optic modulator.

pump laser. This pump laser was then split into two parts. The first part is injected into the highly-nonlinear germanosilicate fiber (FUT: fiber under test) that forms the cavity using an optical circulator (OC). A 90:10 fiber tap coupler was inserted to extract and characterize the BFL signal while the remaining 90% of the Stokes wave was fed back into the passive fiber ring cavity. Note that fiber components used here are made of high-index core single-mode fiber (HI-1060). The Stokes wave makes multiple roundtrips, while the pump laser, which circulates in the opposite direction, is isolated by the OC. The second part of the laser is used to create a beatnote with the BFL. This beatnote is stabilized to an external oscillator via a phase-locking loop (PLL) that feeds back the laser wavelength [17, 18]. This suppresses the thermal drift of our fiber cavity relative to the pump laser. The detected 13.36 GHz beat note signal between the pump laser and the Stokes laser, which corresponds to the Brillouin frequency shift, is then mixed with a Local Oscillator signal provided by an electrical synthesizer whose frequency is set at 13.325 GHz. The mixer output around 33 MHz is fed into a field-programmable gate array (FPGA)-based digital frequency counter and proportional-integrator active digital filter [19]. Finally, the feedback loop is closed by applying the FPGA output signal to the laser diode current. An electrical spectrum analyzer (ESA) is used here to carefully check the single frequency operation of the BFL. The rest of the BFL output is then split into two paths. The first part is sent into an optical spectrum analyzer (OSA, Yokogawa AQ6370) with a resolution of 4 GHz for spectral characterization of stokes lasing. The second part is sent to a delayed self-heterodyne detection (SHD) setup to measure the coherence properties of the BFL. Finally, a heterodyne detection based on a beatnote between an auxiliary laser operating around 1.064 µm and our BFL has been performed, in order to validate our coherence measurements independently.

3. BRILLOUIN SCATTERING CHARACTERIZATION

In order to optimize our fiber cavity, we present the characterized SBS properties of three germanosilicate fibers compatible for an all-fiber configuration with standard single-mode fiber at 1 µm, namely a standard fiber (3.6% mol, SMF-28), a highly nonlinear fiber from Sumitomo Electrics (21% mol, HNLF-1), and a heavily doped-core fiber (75% mol, HNLF-2) from the Fiber Optic Research Center (FORC, Russia).

We measured the experimental SBS threshold (P_{th}) at 1.06 µm pump wavelength in two long fiber samples available, namely a 1.5-km-long segment of SMF-28 fiber and a 0.38-km-long segment of HNLF-1 fiber. The backscattered Stokes wave power as a function of the injected pump power, are shown in Fig. 2(a). In both cases, we first observe the spontaneous Brillouin scattering regime, where the Stokes power increases linearly with the pump power, followed by a transition to the stimulated regime, characterized by a faster increase. We define the Brillouin threshold power as the input power for which the backscattered power reaches 1% of the injected pump power [20], which is equal to 17.2 dBm in the SMF-28 fiber and 15 dBm in the HNLF-1 fiber. These experimental data are very close to the analytically-estimated single-pass SBS threshold values (16.55 and 16.86 dBm for SMF-28 and HNLF-1 fiber respectively, see Eq. 1). A clear difference of 2.2 dB is experimentally observed, while the first sample (SMF-28) is about 4 times longer than the second one (HNLF-1) showing a better opto-acoustic coupling efficiency in the latter case [21]. It worth noting that the Brillouin threshold could not be reached experimentally in the HNLF-2 fiber (see Fig. 2 (a)). In fact, the short fiber length (20 m), implies a high threshold power, which is beyond our maximum available pump power of 250 mW (23.97 dBm, recorded after the port 2 of the optical circulator) at 1 µm wavelength. However, the theoretical single-pass Brillouin threshold value of this specific HNLF-2 fiber was estimated at 26.3 dBm (426.58 mW) based on the following equation [1, 22, 23]:

$$P_{\mathrm{th}} = \frac{21 A_{\mathrm{eff}} K}{g_B L_{\mathrm{eff}}}, \qquad (1)$$

where, K = 1.5 is the polarization factor, $L_{\mathrm{eff}} = (1 - e^{-\alpha L})/\alpha$ the effective fiber length, α the linear fiber loss, A_{eff} the effective mode area, and g_B is the Brillouin gain coefficient.

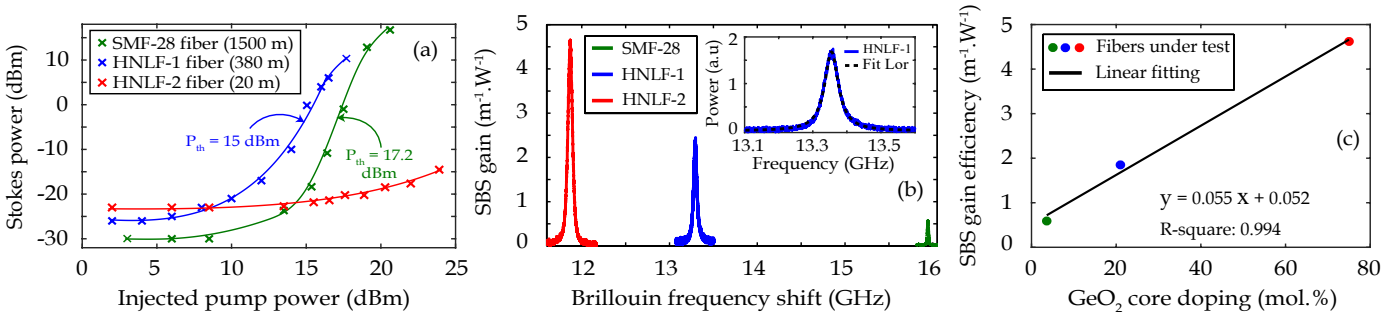

Fig. 2. (a) Experimental measurement backscattered Stokes powers as a function of the injected pump power for standard single-mode silica optical fiber (SMF-28) and high nonlinear silica fibers (HNLF-1, 21 mol. % GeO_2 and HNLF-2, 75 mol. % GeO_2). (b) Experimental Brillouin spectra measured at 1.06 µm in three single-mode germanosilicate core fibers namely SMF-28 (21 mol. % GeO_2), HNLF-1 (21 mol. % GeO_2) and HNLF-2 (75 mol. % GeO_2). Inset: Example of experimental spontaneous backward Brillouin spectrum (blue curve) measured in HNLF-1 fiber and corresponding fit with a Lorentzian curve. (c) SBS gain efficiency as a function of GeO_2 core content.

The BFS ν_B and the Brillouin gain bandwidth $\Delta\nu_B$ were experimentally measured at 1.06 µm in the spontaneous regime (well below the Brillouin critical power threshold) by using a standard heterodyne detection technique, as described in Ref [24]. We characterized our three distinct germanosilicate core fibers as a function of the GeO_2 content (SMF-28: green line; HNLF-1: blue line; HNLF-2: red line). As can be clearly seen in Fig. 2 (b), the BFS strongly reduces from 15.95 GHz down to 11.87 GHz when increasing the GeO_2 content in the fiber core. Indeed, the GeO_2-doping level strongly changes the elastic properties such as the phonon velocity, Young's modulus, and the mass density [25]. As a result, the longitudinal acoustic velocity decreases sharply, which affects the BFS owing to the phase matching relationship [1]. The Brillouin spectral linewidth, obtained with a Lorentzian fit, as shown in the inset of Fig. 2 (b), also increases from 20.5 MHz up to 69.7 MHz with doping, due to the drastic reduction of the acoustic phonon lifetime [26].

Next, the Brillouin gain coefficient, which depends on pumping wavelength, index guiding features, and material properties, of the germanosilicate fibers under test can be estimated by means the following equation [1, 23]:

$$g_B = \frac{2\pi n_{\text{eff}}^7 p_{12}^2}{c\lambda^2 \rho v_A \Delta\nu_B}, \quad (2)$$

where c is the velocity of light, p_{12} is the photo-elastic constant of the glass material, ρ is the material density, and $\Delta\nu_B$ is the full width at half-maximum of the Brillouin gain spectrum. The spectral width $\Delta\nu_B$ is related to the phonon lifetime $T_B = \frac{1}{\pi\Delta\nu_B}$. Taking into account the effective mode area of the three distinct fibers, the estimated SBS gain efficiency (g_B/A_{eff}) increases strongly from 0.59 $W^{-1}\,m^{-1}$ (SMF-28 fiber) up to 4.62 $W^{-1}\,m^{-1}$ (HNLF-2 fiber) at 1-µm as shown in Fig. 2 (c), indicating better opto-acoustic confinement in these fibers [21]. Indeed, increasing the core doping level significantly reduces the effective mode area A_{eff}, which increases the Brillouin gain into the fiber. Table 1 summarizes both opto-geometric and SBS characterization results for all fiber samples under test. Taking into account the SBS characteristics and opto-geometric properties of the fibers studied for their integration with single-mode fiber components operating in the near 1-µm spectral region, it appears that the HNLF-1 fiber with 21% mol GeO_2 is the most suitable for building a Brillouin laser.

Table 1. SBS characterization of three distinct GeO_2-doped core fibers at 1 µm wavelength

Fiber (GeO_2 mol %)	SMF-28	HNLF-1	HNLF-2
Core diameter, ϕ (µm)	8.2	3.6	2.3
Fiber loss, α (dB km^{-1})	1.1	4.8	100
Effective area, A_{eff} (μm^2)	55	8.5	3.5
Fiber length, L (m)	1500	380	20
SBS freq. shift, ν_B (GHz)	15.95	13.36	11.87
SBS bandwidth, $\Delta\nu_B$ (MHz)	20.5	48.7	69.7
SBS gain, $\frac{g_B}{A_{\text{eff}}}$ ($W^{-1}\,m^{-1}$)	0.59	1.85	4.62
SBS threshold, P_{th} (dBm)	17.2 (16.55*)	15 (16.86*)	26.3*

* Analytically-estimated single-pass SBS threshold

4. BRILLOUIN LASER RESULTS

Next, we implemented the BFL cavity with a 15-m-long segment of HNLF-1 fiber. The fiber length was chosen as a trade-off between the gain-loss balance in the ring cavity and the number of cavity modes. The cavity finesse f was estimated to be around 3.3 based on the total cavity losses of 3 dB. The cavity free spectral range (FSR) is calculated to be 12.8 MHz based on the total cavity length.

We then characterized the output signal of the corresponding BFL. In Fig. 3, we show the Stokes power as a function of the input pump power for HNLF-1 fiber with lasing threshold of 140 mW. The inset of figure 3 shows the evolution of the BFL spectra operating around 1 µm, while increasing the pump power from 30 to 200 mW. Note that the pump power is measured at port 1 of the OC. Below the Stokes lasing operation, we clearly see the presence of reflected pump mainly coming from both Fresnel reflections and Rayleigh scattering. By increasing the injected power, the Stokes lasing occurs (blue spectrum) as an upper wavelength shift of 50 pm that matches the SBS frequency and thus confirms that the Brillouin gain is strong enough to compensate the ring cavity losses beyond the threshold. For higher input powers, the first Stokes wave grows significantly and can generate a second-order Stokes wave.

Fig. 4 (a) shows the spectrogram of the beatnote frequency between the Brillouin laser and the pump source, when the PLL is both disabled and active. Without locking, the thermal drift

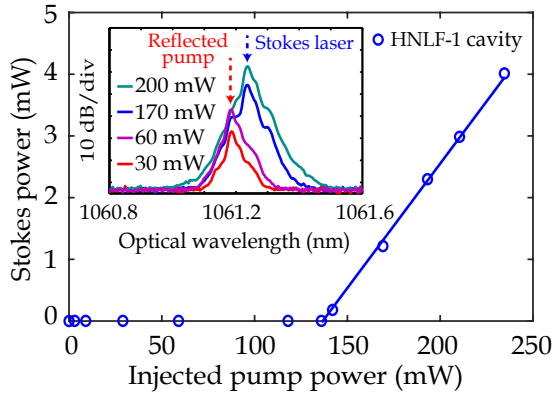

Fig. 3. Stokes lasing threshold measurement of HNLF-1 (15-m long segment, blue circle). Inset: Experimental BFL optical spectra dynamics with the HNLF-1 fiber by varying injected pump power.

of the fiber ring cavity relative to pump laser leads to rapid mode hopping, multimode and unstable emission of Stokes lasing frequency. Note that mode hopping is clearly visible when the Stokes frequency emission switches from one longitudinal mode to another, stepping by one cavity FSR. Activating the PLL to stabilize the beat note maintains a stable single-frequency Brillouin laser without mode hopping. In Fig. 4 (b), we show the beating signal between the pump source and BFL recorded with 51 kHz of resolution bandwidth with an excellent coherent single-frequency lasing emission. We underline that, in our experiment, no mode hopping was observed at any injected pump power during the measurement [17]. We further investigated the coherence properties of our BFL. The linewidth of a BFL can be theoretically estimated using the following equation [27]:

$$\Delta\nu_{\mathrm{BFL}} = \frac{\Delta\nu_{\mathrm{Pump}}}{(1+\frac{\pi\Delta\nu_B}{\frac{c}{nL}\ln(\frac{1}{R})})^2} \quad (3)$$

where $\Delta\nu_{\mathrm{BFL}}$, $\Delta\nu_{\mathrm{Pump}}$, $\Delta\nu_B$, c, n, L and R are the linewidths of the Brillouin and pump lasers, the SBS linewidth, the speed of light, the refractive index, the fiber length, and the cavity feedback parameter, respectively. Using Eq. (3), we can expect a 23 dB narrowing of the BFL linewidth compared to the pump laser. The phase and frequency noises of both BFL and pump laser were also characterized afterward, based on the SHD interferometer and a digital RF coherent receiver [28]. A short delay line of 7.32 µs (corresponding to the fiber length of 1.5-km) which is less than the coherence time of the laser was here used. In this configuration, the system operates in coherent mode [29, 30] and the phase fluctuations of the laser were measured by recording the power spectral density (PSD) using RF analyzer. The frequency noises of the pump laser and HNLF-1 BFL were added on the same plot as described in Fig. 4 (c). Importantly, the interferometer frequency response on the phase noise PSD measurements was removed by using a simple numerical filtering approach developed in Ref [31]. The measurement noise floor was characterized by measuring the frequency noise of the voltage-controlled oscillator driving the AOM (black curve). Across the measurement range, the BFL frequency noise (blue curve) exhibits a stark reduction compared to that of the pump laser (red curve), which reflects the typical linewidth narrowing of the Brillouin effect. Note that the pump laser noise was measured with the PLL disabled. To estimate the integrated linewidth of the BFL and pump laser from the noise measurements, we used the common beta-separation line criterion [32]. This line separates high and low modulation index areas in the frequency noise PSD, which distinguishes contributions to the linewidth versus the wings of the RF line shape. It worth noting that, the beta separation line is an integrated linewidth method that accounts for the technical noise. In that case, it is defined over the integration time of the measurement, which was 10 ms corresponding to the lowest Fourier frequency of 100 Hz. An integrated linewidth of $\sim$ 10 kHz was obtained for the initial pump laser. This value was confirmed by another measurement carried out with a 50-km fiber for direct measurement of the spectral width of the pump laser, which provided a value of 15-kHz. In the case of our BFL output, the intersection between the beta-separation line and the Stokes laser frequency noise yields a narrower integrated linewidth of 1 kHz. Note that using Eq. 1, the narrowed BFL linewidth was expected to be about 50 Hz. The discrepancy between our measurement and theoretical prediction of BFL linewidth can be ascribed to the additional technical noise arising from the mechanical fluctuations [27, 33, 34] of our system, which is not isolated nor packaged, as well as the coupling fluctuations of the laser pump power, which is injected using free space optics before the fiber coupler FC1. We believe the fundamental thermal noise of the resonator [33, 35] is not a limiting effect in our case owing to the large size of the cavity.

Another way of characterizing the laser bandwidth, which is more insensitive to technical fluctuations, is to take into account only the background white frequency noise, which yields an intrinsic (Lorentzian) linewidth. The white frequency noise of our Brillouin laser is at a level of 0.38 $\mathrm{Hz^2/Hz}$ which yields a intrinsic (Lorentzian) linewidth of 1.19 Hz [8, 34, 36]. The white noise floor of the pump laser is 700 $\mathrm{Hz^2/Hz}$ corresponding to a intrinsic linewidth of 2.2 kHz. These noise levels thus yield a 32 dB reduction of the frequency noise. This reduction factor is sizably larger than the theoretically predicted value. We can ascribe this phenomenon to the presence of the feedback loop, which further trims the pump laser noise and enhances the narrowing [37]. The fundamental limit of the Brillouin laser linewidth (see eq. (11) in [34], also used in [10]) is estimated at 28 mHz, which suggests that our system is still limited by the pump noise.

We used the low-noise features of our BFL laser as an optical frequency reference to characterize an auxiliary laser operating around 1.06 µm (RIO 0075-5-08-1, 6-kHz linewidth). To this end, an optical beat-note signal between the two lasers was generated, as shown in Fig. 4 (d), and its phase noise was measured and compared with the SHD measurement of the auxiliary laser. Both measurements show a very similar level and evolution of the frequency noise, indicating the heterodyne system validity and that the noise of our BFL is lower and thus does not limit the auxiliary laser characterization.

5. CONCLUSION

To conclude, a stabilized single-frequency Brillouin narrow-linewidth laser has been demonstrated at 1.06 µm wavelength using a short length of highly GeO_2-doped-core silica fiber. The SBS characterization shows a strong enhancement of the Brillouin gain efficiency in such fibers, thus enabling a BFL threshold of 140 mW with our passive ring cavity, while the resulting BFL linewidth is found to be sub-kHz. Moreover, the significant phase noise reduction of the lasing Stokes component, compared to that of the initial pump laser, is also confirmed. Our mode-

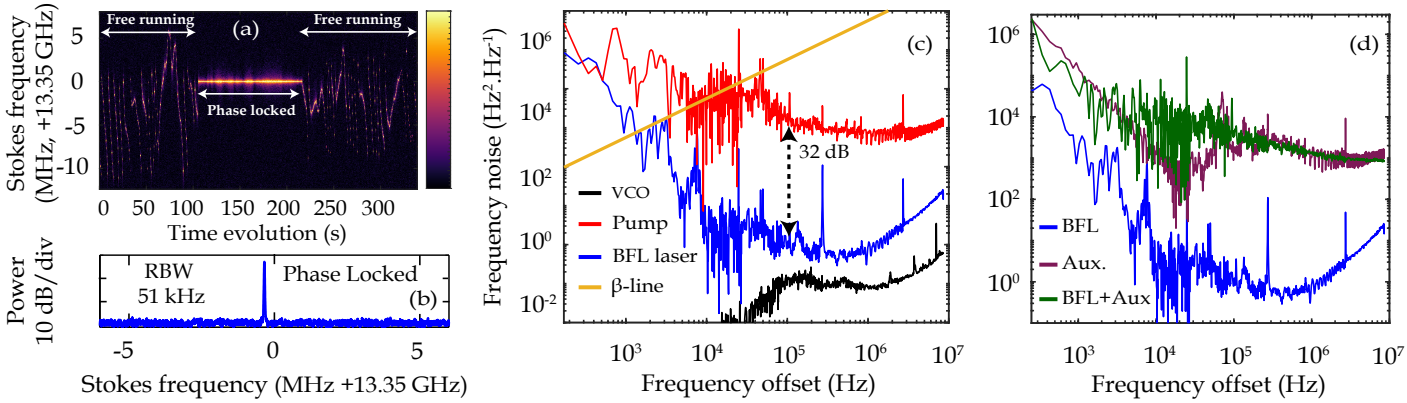

Fig. 4. (a) Spectrogram of relative Stokes laser recorded with 51 kHz resolution bandwidth. (b) Excellent coherent single frequency Stokes emission in phase-locked configuration. (c) Frequency noise of the voltage-controlled reference oscillator (VCO) of AOM, pump source, BFL and auxiliary laser source. The β-separation (solid line, in yellow) shows the intersection with the frequency noise curves, useful for estimating the integrated linewidth. (d) Comparison of Stokes laser frequency noise with auxiliary laser and beat-note noise.

hop free BFL is tunable over the full wavelength range of the pump laser (here, nearly 40 nm). We believe that this low-noise, narrow-linewidth BFL is a promising laser source to provide low-noise reference laser in the spectral region near 1-µm using affordable fiber components and to generate Brillouin-Kerr frequency comb [38].

Funding. The authors acknowledge support from French program "Investments for the Future" operated by the National Research Agency (EIPHI Graduate School, contract ANR-17-EURE-0002), and from Région Bourgogne Franche-Comté and European Regional Development Fund (FEDER).

Disclosures. The authors declare no conflicts of interest.

REFERENCES

1. G. P. Agrawal, *Nonlinear Fiber Optics 6th ed.* (Academic Press, 2019).
2. E. P. Ippen and R. H. Stolen, "Stimulated Brillouin scattering in optical fibers," Appl. Phys. Lett. **21**, 539–541 (1972).
3. K. O. Hill, B. S. Kawasaki, and D. C. Johnson, "cw Brillouin laser," Appl. Phys. Lett. **28**, 608–609 (1976).
4. K. H. Tow, Y. Léguillon, S. Fresnel, P. Besnard, L. Brilland, D. Méchin, D. Trégoat, J. Troles, and P. Toupin, "Linewidth-narrowing and intensity noise reduction of the 2nd order Stokes component of a low threshold Brillouin laser made of Ge10As22Se68 chalcogenide fiber," Opt. Express **20**, B104–B109 (2012).
5. M. Merklein, B. Stiller, K. Vu, S. J. Madden, and B. J. Eggleton, "A chip-integrated coherent photonic-phononic memory," Nat. Commun. **8**, 574 (2017).
6. S. M. Foaleng, M. Tur, J.-C. Beugnot, and L. Thévenaz, "High Spatial and Spectral Resolution Long-Range Sensing Using Brillouin Echoes," J. Light. Technol. **28**, 2993–3003 (2010).
7. C. A. Galindez-Jamioy and J. M. Lopez-Higuera, "Brillouin distributed fiber sensors: an overview and applications," J. Sensors **20170–20180** (2012).
8. S. Gundavarapu, G. M. Brodnik, M. Puckett, T. Huffman, D. Bose, R. Behunin, J. Wu, T. Qiu, C. Pinho, N. Chauhan, J. Nohava, P. T. Rakich, K. D. Nelson, M. Salit, and D. J. Blumenthal, "Sub-hertz fundamental linewidth photonic integrated Brillouin laser," Nat. Photonics **13**, 60 (2019).
9. W. Loh, A. A. S. Green, F. N. Baynes, D. C. Cole, F. J. Quinlan, H. Lee, K. J. Vahala, S. B. Papp, and S. A. Diddams, "Dual-microcavity narrow-linewidth Brillouin laser," Optica **2**, 225–232 (2015).
10. W. Loh, S. Yegnanarayanan, F. O'Donnell, and P. W. Juodawlkis, "Ultra-narrow linewidth Brillouin laser with nanokelvin temperature self-referencing," Optica **6**, 152–159 (2019).
11. A. P. Greenberg, G. Prabhakar, and S. Ramachandran, "High resolution spectral metrology leveraging topologically enhanced optical activity in fibers," Nat Commun **11**, 5257 (2020).
12. A. Mazurenko, S. Blatt, F. Huber, M. F. Parsons, C. S. Chiu, G. Ji, D. Greif, and M. Greiner, "Implementation of a stable, high-power optical lattice for quantum gas microscopy," Rev. Sci. Instruments **90**, 033101 (2019).
13. H. Levine, A. Keesling, A. Omran, H. Bernien, S. Schwartz, A. S. Zibrov, M. Endres, M. Greiner, V. Vuletić, and M. D. Lukin, "High-Fidelity Control and Entanglement of Rydberg-Atom Qubits," Phys. Rev. Lett. **121**, 123603 (2018).
14. J. Wang, Y. Hou, Q. Zhang, D. Jin, R. Sun, H. Shi, J. Liu, and P. Wang, "High-power, high signal-to-noise ratio single-frequency 1 µm Brillouin all-fiber laser," Opt. Express **23**, 28978–28984 (2015).
15. Y. Tao, M. Jiang, L. Liu, C. Li, C. Li, P. Zhou, P. Zhou, and Z. Jiang, "Single-polarization single-frequency Brillouin fiber laser that emits almost 5 W of power at 1 µm," Opt. Lett. **47**, 1742–1745 (2022).
16. Y. Tao, M. Jiang, L. Liu, C. Li, P. Zhou, Jiang, and Zongfu, "More than 20 W, high signal-to-noise ratio single-frequency all-polarization-maintaining hybrid Brillouin/Ytterbium fiber laser," J. Light. Technol. pp. 1–6 (2022).
17. G. Danion, L. Frein, D. Bacquet, G. Pillet, S. Molin, L. Morvan, G. Ducournau, M. Vallet, P. Szriftgiser, and M. Alouini, "Mode-hopping suppression in long Brillouin fiber laser with non-resonant pumping," Opt. Lett. **41**, 2362–2365 (2016).
18. G. Danion, M. Vallet, L. Frein, P. Szriftgiser, and M. Alouini, "Brillouin Assisted Optoelectronic Self-Narrowing of Laser Linewidth," IEEE Photonics Technol. Lett. **31**, 975–978 (2019).
19. L. C. Sinclair, J.-D. Deschênes, L. Sonderhouse, W. C. Swann, I. H. Khader, E. Baumann, N. R. Newbury, and I. Coddington, "Invited Article: A compact optically coherent fiber frequency comb," Rev. Sci. Instruments **86**, 081301 (2015).
20. P. Bayvel and P. M. Radmore, "Solutions of the SBS equations in single mode optical fibres and implications for fibre transmission systems," Electron. Lett. **26**, 434–436 (1990).
21. M. Deroh, J.-C. Beugnot, K. Hammani, C. Finot, J. Fatome, F. Smektala, H. Maillotte, T. Sylvestre, and B. Kibler, "Comparative analysis of stimulated Brillouin scattering at 2 µm in various infrared glass-based optical fibers," J. Opt. Soc. Am. B **37**, 3792–3800 (2020).
22. K. Shiraki, M. Ohashi, and M. Tateda, "SBS threshold of a fiber with a Brillouin frequency shift distribution," J. Light. Technol. **14**, 50–57 (1996).
23. A. Kobyakov, M. Sauer, and D. Chowdhury, "Stimulated Brillouin scat-

tering in optical fibers," Adv. Opt. Photon., AOP **2**, 1–59 (2010).
24. J.-C. Beugnot, T. Sylvestre, D. Alasia, H. Maillotte, V. Laude, A. Monteville, L. Provino, N. Traynor, S. F. Mafang, and L. Thévenaz, "Complete experimental characterization of stimulated Brillouin scattering in photonic crystal fiber," Opt. Express **15**, 15517–15522 (2007).
25. M. Niklès, L. Thévenaz, and P. A. Robert, "Brillouin gain spectrum characterization in single-mode optical fibers," J. Light. Technol. **15**, 1842–1851 (1997).
26. K. Ogusu, H. Li, and M. Kitao, "Brillouin-gain coefficients of chalcogenide glasses," J. Opt. Soc. Am. B **21**, 1302–1304 (2004).
27. A. Debut, S. Randoux, and J. Zemmouri, "Linewidth narrowing in Brillouin lasers: Theoretical analysis," Phys. Rev. A **62**, 023803 (2000).
28. L. Richter, H. Mandelberg, M. Kruger, and P. McGrath, "Linewidth determination from self-heterodyne measurements with subcoherence delay times," IEEE J. Quantum Electron. **22**, 2070–2074 (1986).
29. S. Huang, T. Zhu, Z. Cao, M. Liu, M. Deng, J. Liu, and X. Li, "Laser Linewidth Measurement Based on Amplitude Difference Comparison of Coherent Envelope," IEEE Photonics Technol. Lett. **28**, 759–762 (2016).
30. S. Huang, T. Zhu, M. Liu, and W. Huang, "Precise measurement of ultra-narrow laser linewidths using the strong coherent envelope," Sci. Reports **7**, 41988 (2017).
31. O. Llopis, P. H. Merrer, H. Brahimi, K. Saleh, and P. Lacroix, "Phase noise measurement of a narrow linewidth CW laser using delay line approaches," Opt. Lett. **36**, 2713–2715 (2011).
32. G. D. Domenico, S. Schilt, and P. Thomann, "Simple approach to the relation between laser frequency noise and laser line shape," Appl. Opt. **49**, 4801–4807 (2010).
33. J. Li, H. Lee, and K. J. Vahala, "Low-noise Brillouin laser on a chip at 1064 nm," Opt. Lett., OL **39**, 287–290 (2014).
34. J. Li, H. Lee, T. Chen, and K. J. Vahala, "Characterization of a high coherence, Brillouin microcavity laser on silicon," Opt. Express, OE **20**, 20170–20180 (2012).
35. M. L. Gorodetsky and I. S. Grudinin, "Fundamental thermal fluctuations in microspheres," J. Opt. Soc. Am. B, JOSAB **21**, 697–705 (2004).
36. W. Loh, S. B. Papp, and S. A. Diddams, "Noise and dynamics of stimulated-Brillouin-scattering microresonator lasers," Phys. Rev. A **91**, 053843 (2015).
37. G. Danion, M. Vallet, L. Frein, P. Szriftgiser, and M. Alouini, "Brillouin Assisted Optoelectronic Self-Narrowing of Laser Linewidth," IEEE Photonics Technol. Lett. **31**, 975–978 (2019).
38. E. Lucas, M. Deroh, and B. Kibler, "Dynamic Interplay Between Kerr Combs and Brillouin Lasing in Fiber Cavities," (2022). ArXiv:2212.08534 [physics].